DJS Vol. 46 (3)(2023) –pp. 159- 183 ISSN: 1012-5965

Delta Journal of Science

Available online at
https://djs.journals.ekb.eg/

Research Article **Microbiology**

Intra and extra cellular biosynthesis of selenium nanoparticles by unicellular and filamentous selenium tolerant fungi

Mohamed M. Gharieb, Azza M. Soliman, Esraa M. Hassan*

Faculty of Science, Menoufia University, Microbiology Department

***Corresponding author:** Esraa. M. Hassan **email:** esraa.h14@yahoo.com

Received: 5/7/2023 **Accepted:** 2/8/2023

KEY WORDS

Extracellular, Intracellular, SeNps, biosynthesis, Uni cellular, Filamentous Fungi.

ABSTRACT

Fifty fungal isolates (filamentous and uni cellular) were screened for their ability to reduce sodium selenite (Na_2Seo_3). Out of those, twenty eight isolates displayed positive results therefore they were screened for their ability to tolerate higher concentrations of sodium selenite for different incubation periods. The most active three isolates were characterized morphologically and physiologically. They were identified as *Fusarium oxysporum*, *Rhodotorula mucilaginosa* and *Cryptococcus albidus* based on 18S RNA encoding gene. The selenium reduction power by *Fusarium oxysporum* decreased by increasing the selenite concentration, where it reached the maximum value 96.6% of 1mM concentration of sodium selenite with the net dry weight 7.7 mg/ml. However, the reduction power of *Rhodotorula mucilaginosa* and *Cryptococcus albidus* reached the maximum value 99 and 98.8% of 5 and 7mM of sodium selenite with the net dry weight 7.2 and 6.6 mg/ml respectively. It was found that *F. oxysporum* reduced selenite extra cellular while both *R. mucilaginosa* and *C. albidus* reduced it intra cellular. The biosynthesized selenium particles were purified and dried at 40°C, and characterized using UV- Vis spectroscopic, Transmission electron microscopy and Fourier- Transform infrared Spectroscopy (FTIR) analysis; this is to confirm the selenium nanoparticles (Se-NPs) formation. Transmission electron microscopic images explained the formation of monodisperse spherical-selenium nanoparticles in the range of 14 –97 nm with spherical shape. In addition, the resonance peak appeared at 200- 300 nm which corresponds to the particle size of 14-97 nm. Fourier transform infrared spectroscopy confirmed the presence of a protein shell outside the nanoparticles.

Introduction

Selenium is a chemical element with the symbol Se and atomic number 34. It belongs to group 16 in the periodic table. It is a nonmetal (more rarely considered a metalloid) with properties that are intermediate between the elements above and below in the periodic table, sulfur and tellurium, and also has similarities to arsenic. It seldom occurs in its elemental state or as pure ore compounds in Earth's crust. Selenium (from Ancient Greek σελήνη *(selenē)* 'moon') was discovered in 1817 by Jöns Jacob Berzelius, who noted the similarity of the new element to the previously discovered tellurium (named for the Earth). Selenium is present in nature and in organisms as organic and/or inorganic forms. The main organic forms are selenomethionine and selenocysteine. The inorganic forms are selenite (SeO_3^{-2}), selenide (Se^{-2}), selenate (SeO_2^{-4}) and the selenium element (Se) **(Skalickova *et al*., 2017)**.

Selenium (Se) has unusual physical properties such strong optical conductivity, anisotropy of thermal conductivity, and X-ray sensing responses. Selenium is a component of numerous enzymes; it is a crucial chemical element for all living things. **(Combs and Gray, 1998)**. Although the precise mechanism of Se's actions is not fully understood, it is suggested that Se (a major component of seleno proteins) may be responsible for enhanced carcinogen detoxification, antioxidant protection, inhibition of tumor cell invasion, inhibition of angiogenesis, enhanced immune surveillance, and modulation of cell proliferation (cell cycle and apoptosis) **(Knekt *et al*., 1998).**

Se-NPs, which exhibit a far lower risk than selenium, are frequently used as antioxidants **(Dhanjal and Cameotra, 2010)**. And a dietary supplement **(Rajendran, 2013)**. Due to their higher surface-to-volume ratio at the nano-level, the surface of the particles is more exposed which leads to an enhanced activity of selenium more profoundly in the nano-regime. SeNPs show promising potential as cancer therapeutic agents, and drug carriers in biological applications. Several studies have supported their anticancer, antimicrobial, and anti-biofilm properties **(Li *et al*., 2010).**

SeNPs can be made through chemical processes including acid breakdown, catalytic reduction, and precipitation, as well as physical approaches like laser ablation, ultraviolet light, and hydrothermal methods. These

procedures cost a lot of money and have a lot of issues with using dangerous chemicals and operating them at high pressures and temperatures, which further contaminate the environment (**Medina *et al*., 2018)**. Because biogenic manufacturing takes place in benign environments, using eco-friendly systems like bacteria, yeasts, and fungi to create metallic/metalloid nanoparticles is an effective substitute for physicochemical synthesis. This process is incredibly cost-effective and doesn't create any dangerous compounds to the environment **(Zonaro *et al.*, 2017).** Additionally, the distinctive qualities, functionality, and applications of nanomaterials are strongly correlated with the shape, size, and stability of nanoparticles **(Ramya *et al.*, 2018).** Numerous bacteria from various genera have been found to produce both intracellular and extracellular SeNPs **(Ashengroph and Hosseini, 2021).** Reports on the environmentally friendly synthesis of SeNPs utilizing yeasts, however, are scarce.

Plants, grains, cereals, and meat are all potential sources of selenium that can be consumed as part of a healthy diet. Selenium can be accumulated in considerable levels by the yeast *Saccharomyces cerevisiae*, which can then incorporate it into organic molecules. The main selenium-containing molecule in this yeast's protein fraction and whole cells was found to be selenomethionine **(Korhola *et al.*, 1986)**.

Over the past 10 years, there has been an increase in interest in the use of selenium-containing yeast (selenized yeast) as an enriched selenium supplement in human nutrition, and numerous studies have been conducted to improve the synthesis of this yeast with selenium that is organically bound **(Li *et al.*, 2010).**

Some fungi can tolerate high selenium concentrations (selenium tolerant fungi) as they can reduce selenium intra cellularly (*Rhodotorula mucilaginosa &Cryptococcus albidus*) in their vacuole or extracellularly (*Fusarium oxysporum)* in the growing medium and other cannot tolerate high concentrations of selenium due to its toxic effect **(Gharieb *et al.*, 1995)**. *Fusarium oxysporum* is an ascomycete fungus. *F. oxysporum* strains are ubiquitous soil inhabitants that can exist as saprophytes and degrade lignin and complex carbohydrates associated with soil debris. They are pervasive plant endophytes that can colonize plant roots and may even protect plants or form the basis of disease suppression **(Knekt *et al.*, 1998).** *Rhodotorula mucilaginosa* is basidiomycete fungi**,** has high nutritional value and probiotic effects. Glucan and mannan in the cell wall of *R.*

mucilaginosa can enhance the migration and phagocytosis of macrophages and neutrophils, reduce intestinal inflammatory reactions, enhance animal resistance, promote the reproduction of beneficial bacteria, and competitively inhibit the colonization of harmful bacteria. *R. mucilaginosa* products contain many carotenoids and zymochromes **(Aksu and Eren, 2005);** these carotenoids are beneficial to human and animal health **(Mannazzu *et al.*, 2015).** As the precursor of vitamin, A, carotenoids can resist cancer, inhibit gene mutations, and resist the side effects of environment-induced genotoxic agents by regulating cell signaling and gene expression. Carotenoids are also recognized as super antioxidants, which have various health functions, such as enhancing host immunity, demonstrating anti-oxidation and anti-tumor activity, and lowering blood pressure **(Sharma and Ghoshal, 2020).** Current work aimed to highlight the significance role of these yeasts (*Rhodotorula mucilaginosa and Cryptococcus albidus*) in selenium biosynthesis and their capacity to withstand high selenite concentrations in comparison to some filamentous fungi (*Fusarium oxysporum).*

Materials and methods

Isolation of organisms

The fungal isolates studied in this work were isolated from different sources (Soil, air, vegetables, fruits, leaves, flowers, sugar cane bagasse, and dairy products). They were grown on Potato Dextrose Agar (PDA) medium and Czapek Dox Agar (DOX) medium which contained (g/l); Potato extract (Extracted from 200g potato); Dextrose, 20; Agar, 15; chloramphenicol, 0.1.Dox medium containing (g/l); KCl, 0.5; Na_2NO_3, 2; $MgSO_4.7H_2O$, 0.5; K_2HPO_4, 1.0; Sucrose, 30; Ferrous Sulphate, 0.01; Agar, 15; chloramphenicol, 0.1 and the pH was adjusted to 6.5 **Harrigan, (1998).** The isolates were taken different codes according to its origin (s, a, v, f, l, fl, su, d, sa).

Source	Code
Soil	s
Fruit	f
Sugar cane bagasse	su
Flowers	fl
Dairy products	d
Saccharomyces cerevisiae	sa
Air	a
Vegetables	v
Leaves	l

Also, (F) for filamentous fungi and (Y) for uni cellular fungi (yeasts) were used as abbreviated terms.

PDA and DOX agar medium were prepared, autoclaved, poured in sterilized petri dishes and wait to solidify, serial dilution was done from the soil to inoculate the medium by different dilutions (10^{-1} to 10^{-6}). Vegetables, fruits, sugarcane bagasse, flowers and leaves were printed on the medium surface **Harrigan, (1998).** Dairy products were dissolved in distilled sterilized water, then inoculated on the medium surface. Finally, the inoculated petri dishes were incubated at 28±2°C for 7 days. The grown fungal colonies were purified on PDA and DOX Agar medium.

Transformation of selenite to elemental selenium by fungi on solid agar medium

The ability of fungi to withstand selenite and change into elemental Se was evaluated by growing the isolated fungi on Potassium Dihydrogen Phosphate agar (KDP) medium which contained (g/l); Dextrose, 10.0; peptone, 5.0; $MgSO_4.7H_2O$, 0.5; KH_2PO_4, 1.0; Agar, 15.0 as described by **Kurtzman *et al*., (2011).** Sodium selenite (Na_2Seo_3) with concentration 0.19mM added to the medium and then incubated at 28±2°C for 2 days. The fungal tolerance to selenite reduction was indicated visually by formation of red color of elemental selenium Se^0 **(Mashreghi and Shoeibi, 2017)**.

Transformation of selenite to elemental selenium by fungi on broth medium

The isolated fungi which form red color on agar medium were tested by growing them on KDP broth medium at 28±2°C for 2 days in shaking conditions 120 rpm. After 2 days, the flasks amended with different concentrations of sodium selenite (Na_2SeO_3**)** 0.19, 1.0, 3.0, 5.0, 7.0 and then incubated for further intervals (1, 2 and 3) days at the same conditions. Triplicate sets of flasks were used for each isolate. Non inoculated culture medium was used as a control. The isolates classified according to color power from pale orange to dark red during different incubation periods **(Ghosh *et al*., 2008 and Bajaj *et al*., 2012).**

Identification of the most active fungal isolates

Morphological, biochemical and genetic characterization

The most active fungal isolates were morphologically characterized in accordance with **Lodder, (1970) and Barrnett*et al*., (1990)**.The color, margin and elevation of the isolated yeast colonies grown on DOX agar were recorded, and the fungal cells of 3 days - old colonies were also investigated microscopically using 40X objective lens power to determine cell shape, size, budding and spore formation.

The biochemical characterization was performed by VITEK instrument 7.01 and 8.01 software at mycology lab, Alexandria city. There are 46 biochemical tests measuring carbon source utilization, nitrogen source utilization, and enzymatic activities.

The most active isolates were further identified genetically according to 18S RNA at Macrogen Company, Korea. The polymerase chain reaction (PCR) was performed using the Taq polymerase Dr. MAX DNA Polymerase (Doctor Protein, Korea, cat. no. DR00302) **(Zayed *et al.*, 2020),** and deposited in the Culture Collection Ain Shams University (CCASU) (http://www.wfcc.info/ccinfo/detail) and that it is being held in the faculty of pharmacy, Ain Shams University, PO Box 11566, Cairo, Egypt.

Biosynthesis and purification of selenium nanoparticles from the most active fungi strains

Fusarium oxysporum, Rhodotorula mucilaginosa and *Cryptococcus albidus* were grown on DOX broth medium with different concentrations of sodium selenite. 1.0 ml of each yeast suspension (0.1OD) at 650 nm. were grown in 250 Erlenmeyer flasks containing 50ml medium. While 2 mm disc using sterilized cork porer of pure *Fusarium* culture grown in 250 Erlenmeyer flasks containing 100ml medium. The flasks were incubated at 28± 2ºC for 2 days in shaking conditions 120 rpm. After 2 days, different concentrations of sodium selenite Na_2SeO_3 (1, 3, 5, 7, 10 mM) were added to the flasks and then incubated for 2 days at the same conditions **(Avendano *et al.*, 2016).** Triplicate sets of flasks were used for each fungal strain and sodium selenite concentrations. Selenium free culture medium was used as control. After incubation period, we noted that *F. oxysporum* can reduce sodium selenite extracellulary while *R. mucilaginosa* and *C. albidus* reduce sodium selenite intracellulary. The flasks of *F. oxysporum* were filtered using colander to separate the biomass then the media containing reduced selenium were filtered through filter paper and then centrifuged at 7000 rpm for 30 minutes under cooling conditions 4ºC to obtain SeNps. While the cells of *R. mucilaginosa* and *C. albidus* were digested by sonicator for 20 min to release SeNps to the media, after that the media with the released nano particles kept at 4ºC for 7 days until the large particles precipitate and the small particles remain suspended (supernatant), then the supernatant was centrifuged at 4000 rpm for 15 min to be sure that is free from any yeast residues. After that the harvested supernatant containing SeNps was centrifuged at

7000 rpm for 30 minutes under cooling conditions 4ºC to obtain SeNps. The supernatant of three strains removed and then SeNps pellets were washed three times with deionized water and then 3x with methanol 70% and finally 3x with ethanol 70%, with each washing step the SeNps pellets were vortexed for 5-10 seconds. In this step the impurities were primarily transferred to supernatant while the remaining pellets were composed mainly of selenium nanoparticles. After which the remaining pellets were dried at 40°C.

The net dry weight of each fungi were calculated and the percentage of selenite reduction was determined by inductively coupled plasma mass spectroscopy(ICP-MS) instrument at Genetic Engineering and Biotechnology Research Institute, Sadat city, Menoufia, Egypt. To reveal the extent of selenite reduction, the reduction efficiency of selenite (E_1) was defined and calculated as following equation:

$E_1 = (SeO_3)^{-2}{}_c - (SeO_3)^{-2}{}_t \;/\; (SeO_3)^{-2}{}_c \times 100\%$

where $(SeO_3)^{-2}{}_c$ and $(SeO_3)^{-2}{}_t$ were the concentrations of unreduced selenium in control and treated, respectively as described by **(Xinzhang *et al*., 2020)**.

Characterizations of SeNPs

1- Detection using UV-Vis spectroscopy

For UV-Vis spectroscopic investigation of the nanoparticles, 2 mL of a fungal solution containing selenium nanoparticles was placed in a cuvette. The absorbance was recorded by UV Vis spectroscopy between 200 to 1200nm. The absorbance at which the peak was formed was noted (200-300nm) **(Singh *et al*., 2014).**

2- Transmission Electron Microscope (TEM) analysis

At the National Research Centre in Cairo, Egypt, the TEM investigation was also carried out on the recovered pellets of selenium nanoparticles to ascertain the morphology and size of SeNPs. For this, a 20-minute sonication process using an ultrasonicator (made by Crest Ultrasonics Corp., New Jersey, USA) was performed on a fungal solution containing selenium nanoparticles. A few droplets were then put onto a copper grid that had been coated with carbon before being allowed to dry. The grid was then analyzed using HR-TEM (JEOL, JEM-2100, Tokyo, Japan), which was run at 200 kv **(Singh *et al*., 2014).**

3-Fourier-transform infrared spectroscopy (FTIR) analysis

The selenium nanoparticle pellets were examined after being cleaned and dried in an oven at 40°C. Fourier transform infrared spectroscopy (Jasco FTIR 6100 Japan) was used to record all spectra (61 spectra) with wave numbers between 4500 and 500cm^{-1}. OPUS (version 2.2) from Bruker was utilized for data

processing and sample identification. All spectra were vector normalized and base line adjusted. A 4 cm^{-1} spectral resolution was chosen **(Salem *et al.*, 2010).**

Statistical analysis

The values given in this study were the means of three replicates and were expressed as means standard error (SE) of the mean before being subjected to one- and two-way analysis of variance (ANOVA) to ascertain the level of significance for the changes achieved by the applied treatments. Additionally, correlation coefficients were used to examine the significance of the connections between the fungi's examined factors. The analysis was carried out by Info stat statistical program 2020, where, $P \geq 0.05$= Nonsignificant, $P \leq 0.05$= Significant, $P \leq 0.01$= highly significant.

Results

Isolation and screening the fungal isolates on solid agar and broth medium:

Fifty fungal isolates were isolated from different sources (soil, air, vegetables, fruits, leaves, flowers, sugar cane bagasse, dairy products and *saccharomyces cerevisiae*). The isolates taken different codes (s, a, v, f, l, fl, su, d, sa), respectively. (F) for filamentous fungi isolates and (Y) for uni cellular fungi isolates (yeasts). There are 30 yeast isolates and 20 filamentous fungi isolates. The isolates were purified on PDA and Dox agar medium then screened on Potassium Di hydrogen Phosphate agar medium supplemented with 0.19mM sodium selenite (Fig. 1). We found that 28 fungal isolates have the ability to reduce sodium selenite to elemental selenium by the formation of red color, while 22 isolates could not form such a color (Table 1). After screening on solid agar medium, the 28 fungal active isolates were screened on KDP broth medium supplemented with different concentrations of sodium selenite (0.19, 1.0, 3.0, 5.0, 7.0) mM for more different incubation periods (1, 2& 3) days in shaking conditions 120 rpm. The isolates classified according to color power from pale orange to dark red during the incubation intervals. (Table 2) indicates that Yl_6, Yv_{10}& Fv_9 are the most active fungal isolates that capable of reducing sodium selenite at high concentrations (5.0, 7.0) mM after 2 days of incubation (Fig. 2). WhileYl_6, Yv_{10} were the unicellular fungi (yeasts) isolated from leaves and vegetables respectively, and the isolate Fv_9 was multicellular fungi isolated from vegetables.

Table (1): Screening the fungal isolates on solid agar medium

Fungal isolates	Selenium reduction tolerance	Fungal isolates	Selenium reduction tolerance
Ys_1	+	Yd_{26}	_
Ys_2	+	Yfl_{27}	+
Ys_3	_	Yfl_{28}	+
Yl_4	_	Yfl_{29}	_
Yl_5	_	Ysa_{30}	_
Yl_6	+	Fs_1	_
Yv_7	+	Fs_2	+
Yv_8	_	Fs_3	+
Yv_9	_	Fs_4	_
Yv_{10}	+	Fa_5	_
Yv_{11}	+	Fl_6	_
Yv_{12}	+	Fl_7	+
Yf_{13}	+	Fl_8	+
Yf_{14}	_	Fv_9	+
Yf_{15}	_	Fv_{10}	_
Yf_{16}	+	Fv_{11}	+
Yf_{17}	_	Fv_{12}	+
Ya_{18}	+	Ff_{13}	_
Ya_{19}	_	Ff_{14}	+
Ya_{20}	_	Ff_{15}	+
Ysu_{21}	+	Fsu_{16}	+
Ysu_{22}	+	Fsu_{17}	+
Ysu_{23}	+	Ffl_{18}	_
Ysu_{24}	_	Ffl_{19}	+
Yd_{25}	_	Ffl_{20}	+

Table (2): Screening the fungal isolates on broth medium

Isolates	Sodium selenite concentrations(mm)														
	0.19			1			3			5			7		
	Reduction selenium/ day			Reduction selenium/ day			Reduction selenium/ day			Reduction selenium/ day			Reduction selenium/ day		
	1	2	3	1	2	3	1	2	3	1	2	3	1	2	3
Yl_6	++	+++	+++	++	+++	+++	++	+++	+++	+++	++++	++++	+++	++++	++++
Yv_{10}	++	+++	+++	++	+++	+++	++	+++	+++	+++	++++	++++	+++	++++	++++
Fv_9	++	+++	+++	++	+++	+++	++	+++	+++	+++	++++	++++	+++	++++	++++

Where (++) dark orange , (+++) pale red (++++) dark red

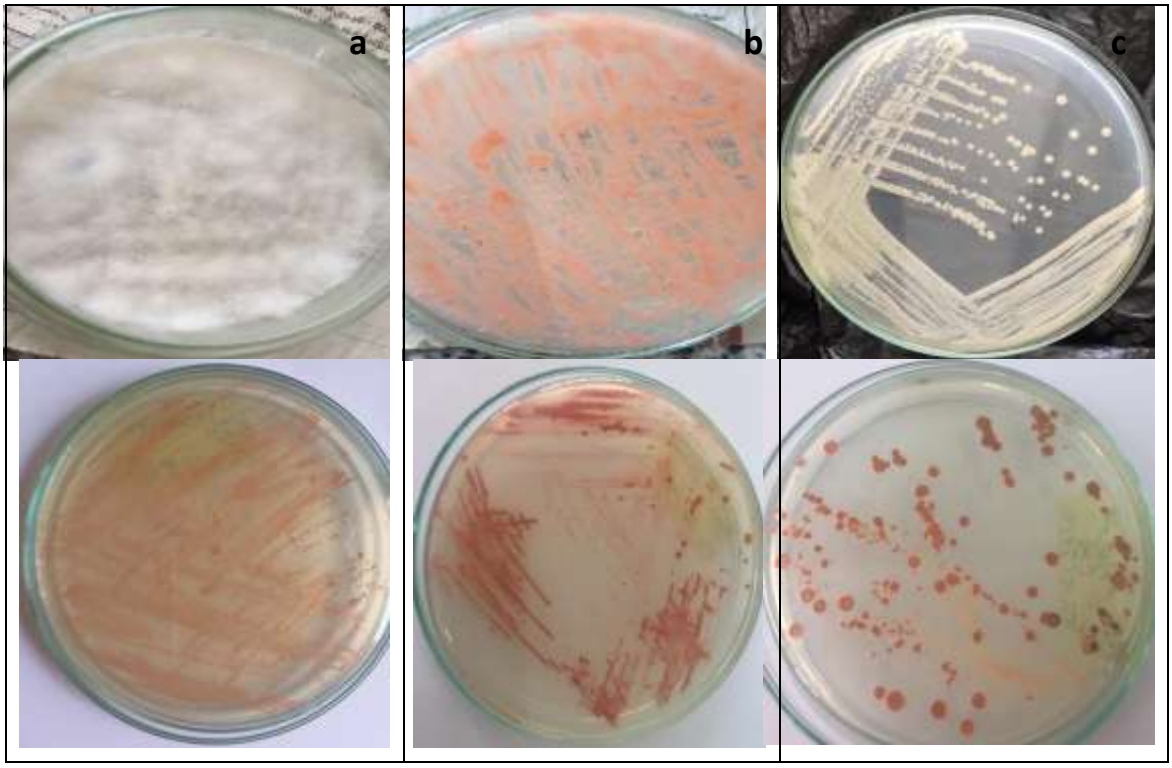

Fig. (1): Photograph shows the transformation of sodium selenite (0.19 mM) into elemental selenium on solid agar medium by (a) $Fv_{9,}$ (b) Yl_6 & (c) Yv_{10} on the lower part and the control plates without sodium selenite on the upper part.

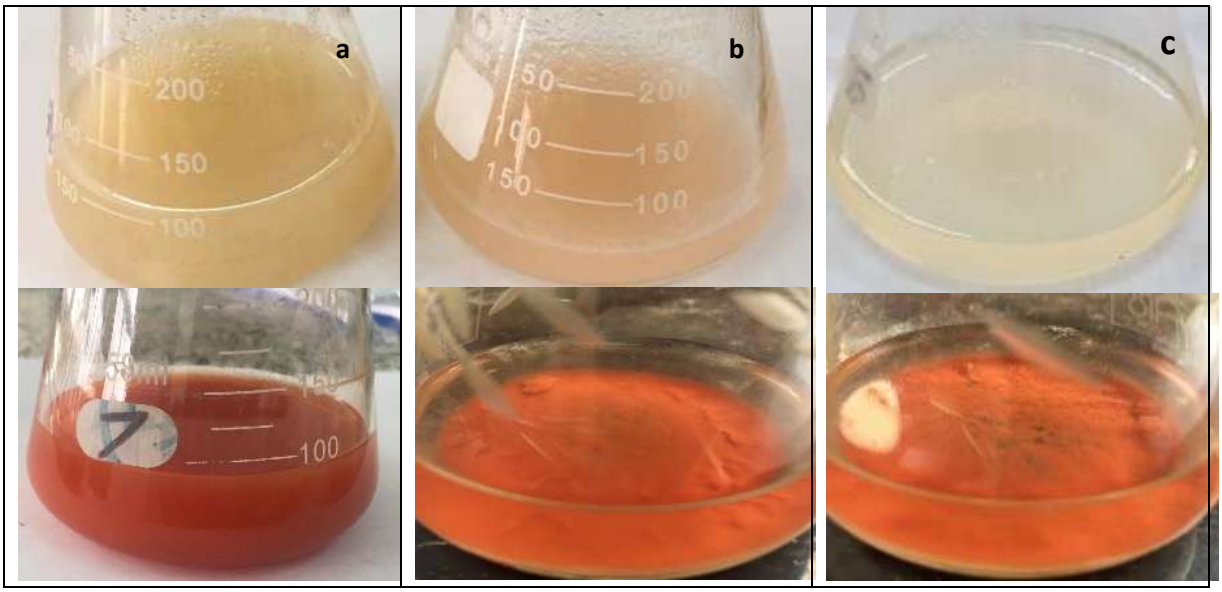

Fig. (2): Photograph shows the transformation of sodium selenite (5mM) into elemental selenium on broth medium by (a) $Fv_{9,}$ (b) Yl_6&(c) Yv_{10} on the lower part and the control flasks without sodium selenite on the upper part.

Morphological, biochemical and genetic characterization of the most active fungal isolates

The Morphological characterization of the yeast isolates (Table 3) described by **Lodder, (1970) and Barrnet*et et al.*, (1990).** While Fv_9 isolate is filamentous fungi has white cottony mycelium with dark purple under surface on growth media and oval to ellipsoid/ kidney shaped oval tapering and three septate spores under light microscope.

The biochemical characterization of the most active yeasts was performed by VITEK instrument. There are 46 biochemical tests measuring carbon source utilization, nitrogen source utilization, and enzymatic activities as indicated in (Table 4&5). Yl_6 was identified as *Rhodotorula mucilaginosa* (94% probability), while Yv_{10} was identified as *Cryptococcus albidus* (90% probability). Biochemical tests abbreviations indicated in (Table 6).

Table (3): Morphological characterization of yeast isolates

Yeast isolates	Cell shape	Color	Size	Margin	Elevation
Yl_6	Ovoid- budding	Orange	Moderate	Entire	Raised
Yv_{10}	Spherical- budding	White to creamy	Moderate	Entire	Raised

Table (4): Biochemical tests of Yl_6

3	LysA	-	**4**	IMLTa	-	**5**	LeuA	+	**7**	ARG	+	**10**	ERYa	-	**12**	GLYLa	-
13	TyrA	-	**14**	BNAG	-	**15**	ARBa	-	**18**	AMYa	-	**19**	dGALa	(-)	**20**	GENa	-
21	dGLUa	+	**23**	LACa	-	**24**	MAdGa	-	**26**	dCELa	-	**27**	GGT	-	**28**	dMALa	-
29	dRAFa	+	**30**	NAGAl	-	**32**	dMNEa	-	**33**	dMELa	-	**34**	dMLZa	-	**38**	ISBEa	-
39	IRHAa	-	**40**	XLTa	+	**42**	dSORa	-	**44**	SACa	(+)	**45**	URE	(-)	**46**	AGLU	-
47	dTURa	-	**48**	dTREa	-	**49**	NO3a	-	**51**	IARAa	-	**52**	dGATa	(+)	**53**	ESC	-
54	IGLTa	+	**55**	dXYLa	-	**56**	LATa	-	**58**	ACEa	+	**59**	CITa	-	**60**	GRTas	(-)
61	IPROa	+	**62**	2KGa	-	**63**	NAGa	-	**64**	dGNTa	(-)						

Table (5): Biochemical tests of Yv_{10}

3	LysA	-	**4**	IMLTa	-	**5**	LeuA	+	**7**	ARG	-	**10**	ERYa	-	**12**	GLYLa	-
13	TyrA	-	**14**	BNAG	-	**15**	ARBa	(+)	**18**	AMYa	-	**19**	dGALa	-	**20**	GENa	+
21	dGLUa	+	**23**	LACa	-	**24**	MAdGa	(-)	**26**	dCELa	-	**27**	GGT	-	**28**	dMALa	+
29	dRAFa	+	**30**	NAGAl	-	**32**	dMNEa	-	**33**	dMELa	-	**34**	dMLZa	+	**38**	ISBEa	-
39	IRHAa	+	**40**	XLTa	+	**42**	dSORa	+	**44**	SACa	+	**45**	URE	+	**46**	AGLU	+
47	dTURa	+	**48**	dTREa	-	**49**	NO3a	+	**51**	IARAa	+	**52**	dGATa	+	**53**	ESC	+
54	IGLTa	+	**55**	dXYLa	+	**56**	LATa	-	**58**	ACEa	+	**59**	CITa	-	**60**	GRTas	+
61	IPROa	+	**62**	2KGa	+	**63**	NAGa	-	**64**	dGNTa	-						

Table (6): Biochemical tests abbreviations

3	L-Lysine-ARYLAMIDASE	LysA	**49**	L-RHAMNOSE assimilation	IRHAa
4	L-MALATE assimilation	IMLTa	**40**	XYLITOL assimilation	XLTa
5	Leucine-ARYLAMIDASE	LeuA	**42**	D-SORBITOL assimilation	dSORa
7	ARGININE	ARG	**44**	SACCHAROSE/SUCROSE assimilation	SACa
10	ERYTHRITOL assimilation	ERYa	**45**	UREASE	URE
12	GLYCEROL assimilation	GLYLa	**46**	ALPHA-GLUCOSIDASE	AGLU
13	Tyrosine ARYLAMIDASE	TyrA	**47**	D-TURANOSE assimilation	dTURa
14	BETA-N-ACETYL-GLUCOSAMINIDASE	BNAG	**48**	D-TREHALOSE assimilation	dTREa
15	ARBUTIN assimilation	ARBa	**49**	NITRATE assimilation	NO3a
18	AMYGDALIN assimilation	AMYa	**51**	L-ARABINOSE assimilation	IARAa
19	D-GALACTOSE assimilation	dGALa	**52**	D-GALACTURONATE assimilation	dGATa
20	GENTOBIOSE assimilation	GENa	**53**	ESCULIN hydrolysis	ESC
21	D-GLUCOSE assimilation	dGLUa	**54**	L-GLUTAMATE assimilation	IGLTa
23	LACTOSE assimilation	LACa	**55**	D-XYLOSE assimilation	dXYLa
24	METHYL-A-D-GLUCOPYRANOSIDE assimilation	MAdGa	**56**	DL-LACTATE assimilation	LATa
26	D-CELLOBIOSE assimilation	dCELa	**58**	ACETATE assimilation	ACEa
27	GAMMA-GLUTAMYL-TRANSFERASE	GGT	**59**	CITRATE (SODIUM) assimilation	CITa
28	D-MALTOSE assimilation	dMALa	**60**	GLUCURONATE ASSIMILATION	GRTas
29	D-RAFFINOSE assimilation	dRAFa	**61**	L-PROLINE assimilation	IPROa
30	PNP-N-acetyl-BD-galactosaminidase 1	NAGA1	**62**	2-KETO-D-GLUCONATE assimilation	2KGa
32	D-MANNOSE assimilation	dMNEa	**63**	N-ACETYL-GLUCOSAMINE assimilation	NAGa
33	D-MELIBIOSE assimilation	dMELa	**64**	D-GLUCONATE assimilation	dGNTa
34	D-MELEZITOSE assimilation	dMLZa			
38	L-SORBOSE assimilation	ISBEa			

Molecular identification of the isolated fungi

In addition to morphological and biochemical identification, the molecular identification of the isolated fungi was performed using 18S RNA encoding gene. The isolate Yl_6 was *Rhodotorula mucilaginosa* strain (GQ433375. 1) 96% homology, while isolate Yv_{10} was *Cryptococcus albidus* strain (AB032617.1) 95% homology and Fv_9 was *Fusarium oxysporum* strain (LT841236.1) 98% homology. The phylogenetic trees of the 3 isolates were shown in Figs. (3, 4 and 5).The strains have been deposited in the Culture Collection Ain Shams University (CCASU) under the following codes: *Fusarium oxysporum*, CCASU-2023-F9, *Rhodotorula mucilaginosa*, CCASU-2023-F10, and *Cryptococcus albidus*, CCASU-2023-F11.

Primer Information

Sequencing Primer Name Primer Sequences	PCR Primer Name Primer Sequences
NS1 5' (GTA GTC ATA TGC TTG TCT C) 3'	NS1 5' (GTA GTC ATA TGC TTG TCT C) 3'
NS24 5' (TCC GCA GGT TCA CCT ACG GA) 3'	NS24 5' (TCC GCA GGT TCA CCT ACG GA) 3'

Subject						Score		Identities	
Accession	Description	Length	Start	End	Coverage	Bit	E-Value	Match/Total	Pct.(%)
LT841236.1	Fusarium oxysporum	7875	68	1718	20	3049	0.0	1651/1651	100

Kingdom	Family	Genus	Species
Eukaryota	Nectriaceae	Fusarium	Fusarium oxysporum

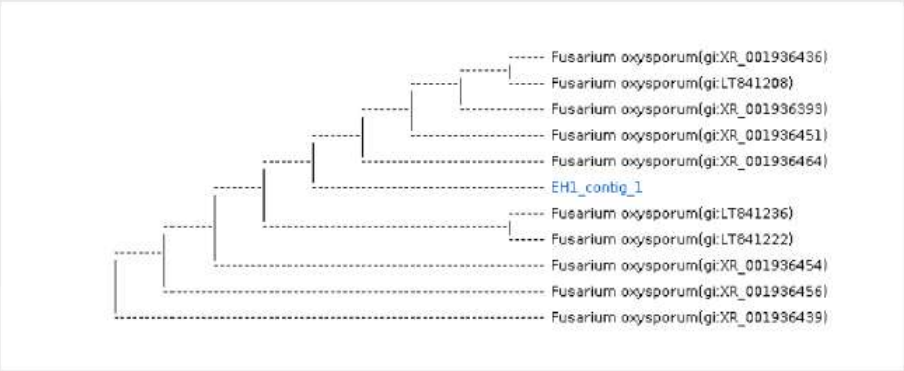

Fig. (3): Phylogenetic tree constructed from 18S RNA sequence of *Fusarium oxysporum* strain (LT841236.1) with primer information.

Primer Information

Sequencing Primer Name Primer Sequences	PCR Primer Name Primer Sequences
NS1 5' (GTA GTC ATA TGC TTG TCT C) 3'	NS1 5' (GTA GTC ATA TGC TTG TCT C) 3'
NS24 5' (TCC GCA GGT TCA CCT ACG GA) 3'	NS24 5' (TCC GCA GGT TCA CCT ACG GA) 3'

Subject						Score		Identities	
Accession	Description	Length	Start	End	Coverage	Bit	E-Value	Match/Total	Pct.(%)
GQ433375.1	Rhodotorula mucilaginosa	1709	34	1696	97	3072	0.0	1663/1663	100

Kingdom	Family	Genus	Species
Eukaryota	Sporidiobolaceae	Rhodotorula	Rhodotorula mucilaginosa

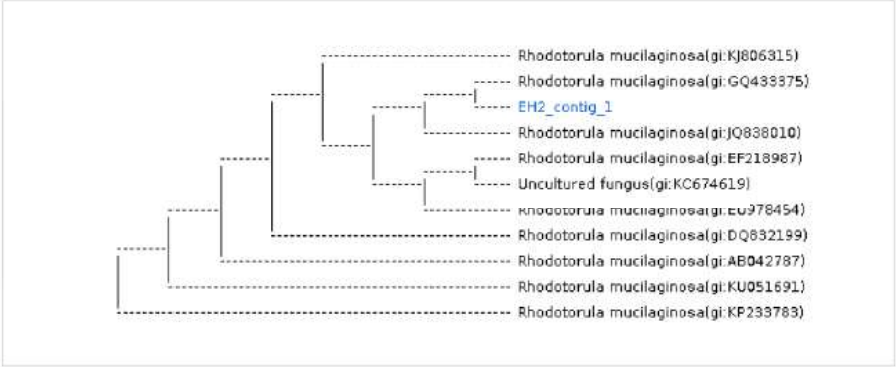

Fig. (4): Phylogenetic tree constructed from 18S RNA sequence of *Rhodotorula mucilaginosa* strain (GQ433375. 1) with primer information.

Primer Information

Sequencing Primer Name Primer Sequences	PCR Primer Name Primer Sequences
NS1 5' (GTA GTC ATA TGC TTG TCT C) 3'	NS1 5' (GTA GTC ATA TGC TTG TCT C) 3'
NS24 5' (TCC GCA GGT TCA CCT ACG GA) 3'	NS24 5' (TCC GCA GGT TCA CCT ACG GA) 3'

Subject						Score		Identities	
Accession	Description	Length	Start	End	Coverage	Bit	E-Value	Match/Total	Pct.(%)
AB032617.1	Cryptococcus albidus	1782	564	1713	64	2030	0.0	1135/1150	99

Kingdom	Family	Genus	Species
Eukaryota	Filobasidiaceae	Naganishia	Cryptococcus albidus

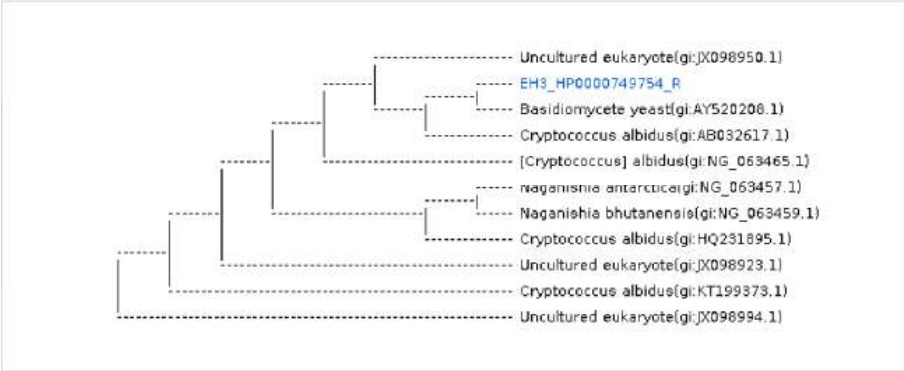

Fig. (5): Phylogenetic tree constructed from 18S RNA sequence of *Cryptococcus albidus* strain (AB032617.1) with primer information.

Biosynthesis of selenium nanoparticles by *Fusarium oxysporum*, *Rhodotorula mucilaginosa* and *Cryptococcus albidus* at different selenite concentrations

Different concentrations of sodium selenite (1.0, 3.0, 5.0, 7.0, 10.0mM) were added to DOX broth medium to determine the tolerance of *F. oxysporum*, *R. mucilaginosa* and *C. albidus* to selenite and the formation of elemental selenium.Table 7 indicates that the reduction power of *F. oxysporum* decreased by increasing the selenite concentration, as it reached the maximum value (96.6%) at 1mM concentration of sodium selenite with the net dry weight of 7.7 mg/ml. However the reduction power of *R. mucilaginosa* and *C. albidus* reached the maximum value (99 & 98.8%) at 5.0& 7.0 mM of sodium selenite with the net dry weight (7.2 & 6.6 mg/ml) respectively. The produced selenium particles were purified and dried at 40°C.

Table (7): Effect of different selenite concentrations on reduction (%) of Na_2SeO_3 by *Fusarium oxysporum*, *Rhodotorula mucilaginosa* and *Cryptococcus albidus* P< 0.0001= highly significant

Fungal strains	Reduction power%				
	Sodium selenite concentrations (mM)				
	1	3	5	7	10
F. oxysporum	96.56±0.59 [a]	42.51±0.39 [a]	26.41±0.56 [a]	15.62±1.83 [a]	9.78±1.59 [a]
R. mucilaginosa	89.00±1.19 [a]	98.39±0.21 [a]	99.09±0.04 [a]	96.21±0.35 [a]	42.86±0.82 [a]
C. albidus.	95.04±0.07 [a]	96.46±0.07 [a]	97.97±0.17 [a]	98.87±0.12 [a]	43.33±0.82 [a]

Detection using UV-Vis spectroscopy

For SeNPs spectra measurements, the UV-Vis spectrum displays an absorption peak in the 200-1200 nm range for the cell filtrate from the culture of fungal strains, and Fig. 6 shows a well-defined absorption peak at 200-300 nm that corresponds to the wavelength of the selenium nanoparticles' surface plasmon resonance (SPR) which is the most outstanding optical property of metallic nanostructures. It consists of a collective oscillation of conduction electrons excited by the electromagnetic field of light.

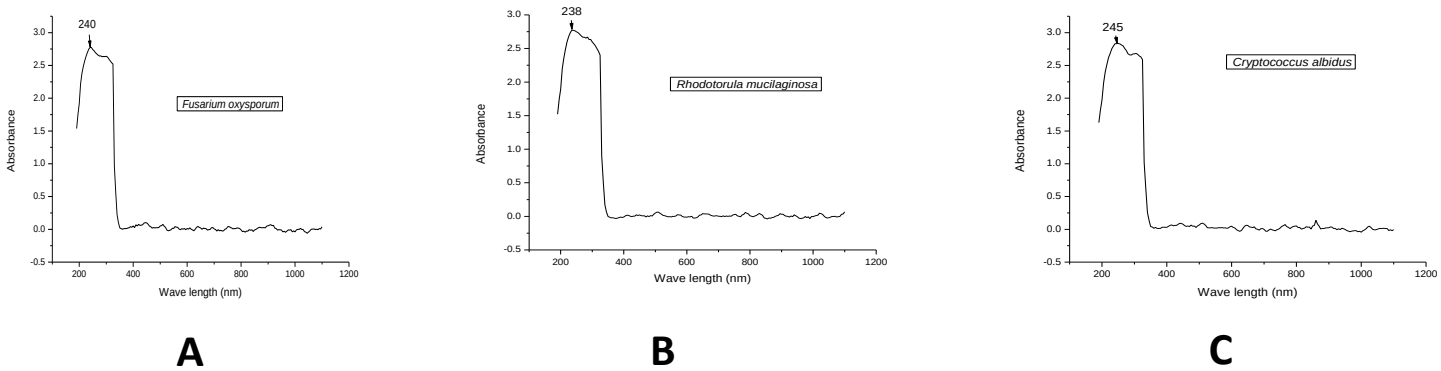

Fig. (6): UV-Vis spectra recorded of selenium nanoparticles produced by the three fungal strains (A) *Fusarium oxysporum*, (B) *Rhodotorula mucilaginosa* and (C) *Cryptococcus albidus*. The absorption spectrum of SeNPs exhibit peak at 240 nm for *F. oxysporum*, 238 and 245 nm for both *R. mucilaginosa* and *C. albidus*.

Transmission Electron Microscopy (TEM)

TEM is very important technique, which is used to get the information about particle size and shape of the synthesized nanoparticles. Transmission electron microscope image of the synthesized selenium nanoparticle are

shown in Figs 7, 8 and 9. Spherical shape of individual nanoparticles, with size in the range of 14–97nm, is evident from the TEM image.

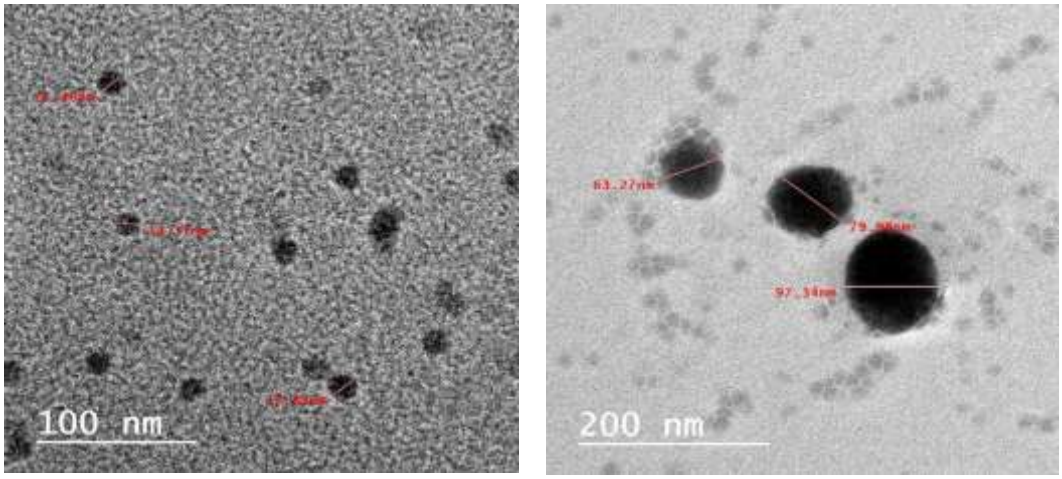

Fig. (7): TEM image of the selenium nanoparticles produced by *Fusarium oxysporum* strain (LT841236.1).

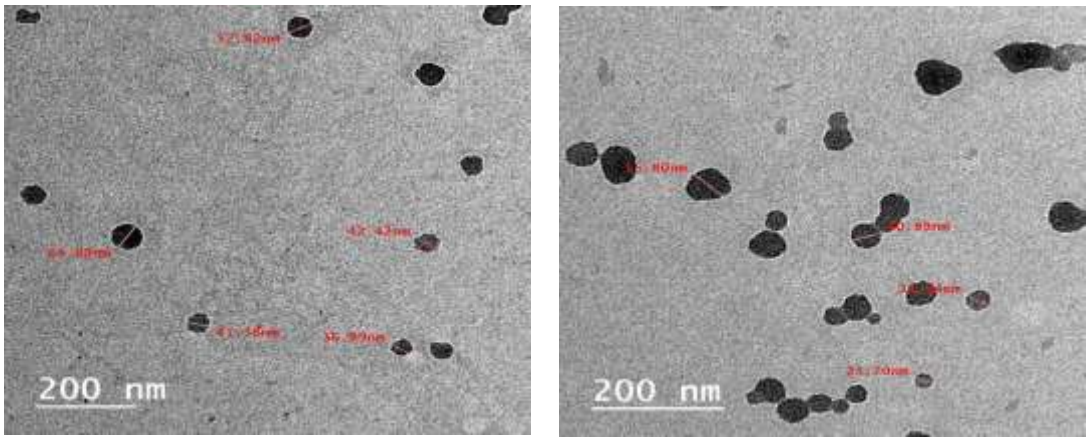

Fig. (8): TEM image of the selenium nanoparticles produced by *Rhodotorula mucilaginosa* strain (GQ433375.1).

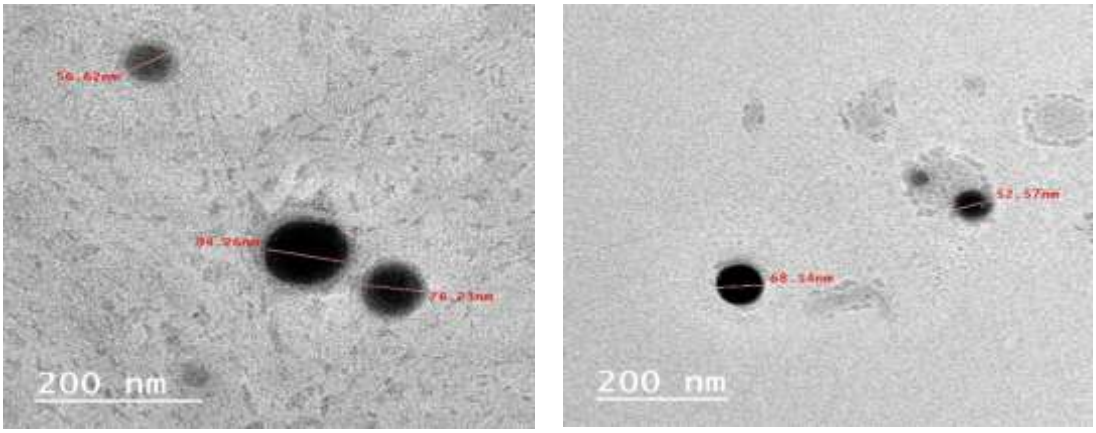

Fig. (9): TEM image of the selenium nanoparticles produced by *Cryptococcus albidus* strain (AB032617.1).

Fourier-transform infrared spectroscopy (FTIR)

Using (FTIR), the three studied stains' biosynthesized SeNPs were identified. The SeNPs' FTIR spectra (figures 10, 11, and 12) revealed many peaks appearance of 581, 593, 2354, and 2851 cm^{-1}, which are indicative of proteins. The hydroxyl (OH) group can be used to explain the strong broad peaks at 3432, 3442, and 3440 cm^{-1}, which correlate to the amine group (NH stretching). With CH stretching, the peaks at 2917 and 2926 cm^{-1} are observed **(Mukherje, 2014).** The bands at 1634, 1640 and 1632 cm^{-1} may be attributed to C-Ostretching mode **(Huang *et al*., 2007)** The peak at 617 cm-1 likely due to thepresence of C−S sulfide stretching vibration **(Tani *et al*., 2007)**. In addition, the FTIR spectra showed bands at 1035, 1936, and 1385 cm-1 that were associated with proteins' amide I. The Amide I band is a C=O stretching mode. Near 1385 cm-1 is where you can find the more intricate Amide III band. The amide groups indicating the presence of enzymes were in charge of the metal ion stabilization and reduction synthesis **(Prasad and Selvaraj, 2014).** This result indicates that molecules with these functional groups are associated with the NPs **(Díaz-Visurraga *et al*., 2012).** With the overall observations, it can be concluded that the proteins might have formed a capping agent over the SeNPs, which may response for their stabilization **(Sonkusre *et al*., 2014).**

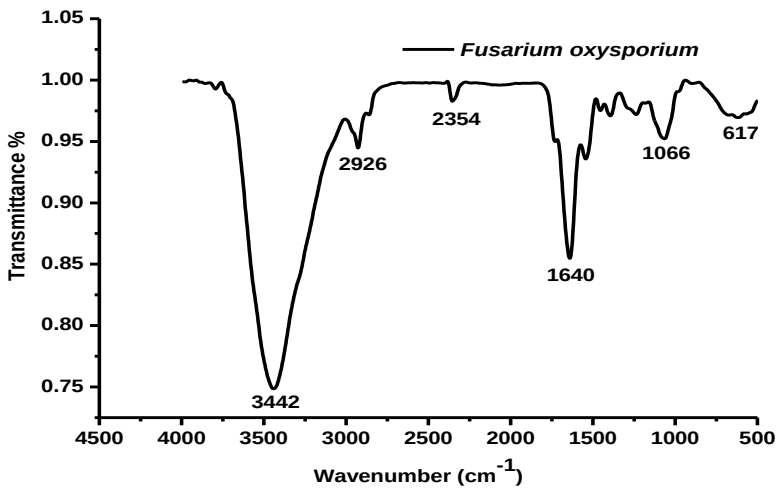

Fig. (10): A representative FTIR spectrum pattern of dried powder of selenium nanoparticles synthesized by *Fusarium oxysporum* (LT841236.1)

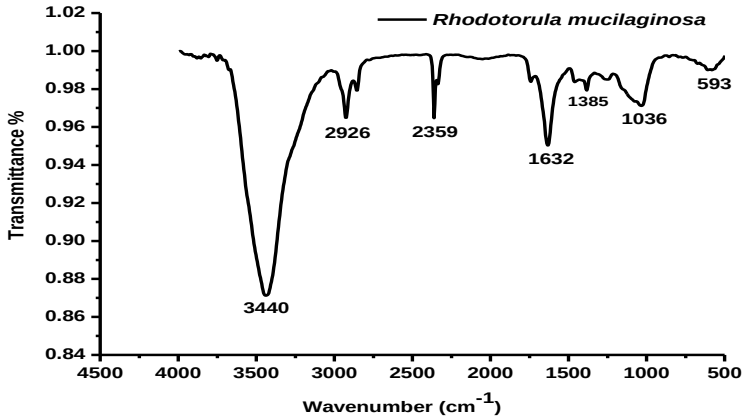

Fig. (11): A representative FTIR spectrum pattern of dried powder of selenium nanoparticles synthesized by *Rhodotorula mucilaginosa* (GQ433375.1)

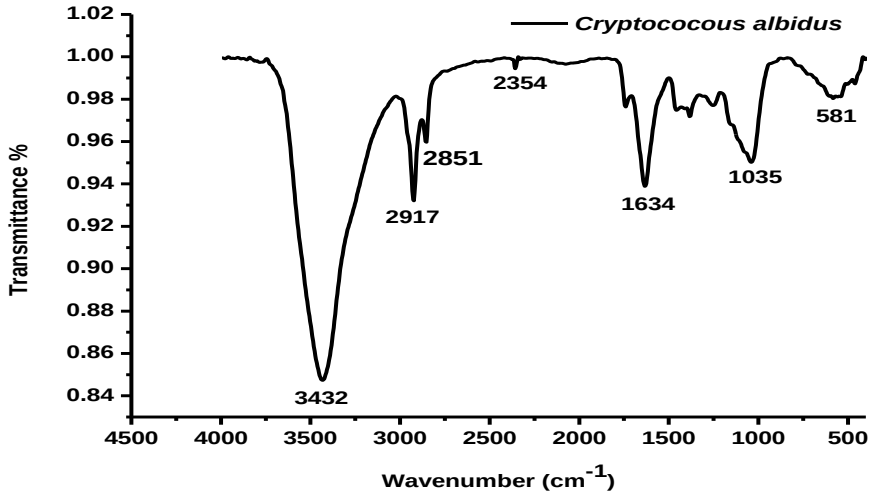

Fig. (12): A representative FTIR spectrum pattern of dried powder of selenium nanoparticles synthesized by *Cryptococcus albidus (*AB032617.1*)*

Discussion

Selenium is very important trace element which is required up to 40–300 µg for human body every day. Only small amount is required for maintaining the function, and a large amount of selenium may be harmful to the human body **(Srivastava *et al.,* 2015)**. It is useful in regulating the function of the human body. It is useful in protecting cardiovascular health, regulating thyroid hormones and immune response, and preventing progression of cancer **(Srivastava *et al.,* 2015)**. Selenium is less toxic and high active of selenium nanoparticles are used in many medical applications such as antitumor **(Ramamurthy *et al.,* 2013)**, antimicrobial **(Bartůněk *et al.,* 2015)** and drug delivery. Selenium has codons in mRNA which form seleno-cysteine by

entering as selenoprotein **(Srivastava *et al*., 2015)**.

In this study, fifty fungal strains were isolated on PDA and DOX agar medium then purified on the same medium. The tolerance of fungi to selenite was tested by growing them on KDP agar medium **(Kurtzman*et al*., 2011)** supplemented with 0.19 mM sodium selenite. The fungal tolerance to selenite was indicated visually by the formation of red color of elemental selenium Se^0 **(Mohammed and Sara, 2017)**. Twenty eight fungal isolates displayed the ability to reduce selenite, so they were screened on KDP broth medium supplemented with different concentrations of sodium selenite for different incubation periods. The isolates were classified according to color power from pale orange to dark red during different incubation time intervals **Ghosh *et al*., 2008 and Bajaj *et al*., 2012.** The most active fungal strains were characterized morphologically based on **Lodder, 1970 and Barrnett*et al*., 1990**. Then biochemically and finally identified genetically on the bases of 18S RNA **(Zayed *et al*., 2020)** as *F. oxysporum, R.mucilaginosa and C.albidus.* The Effect of different selenium concentrations on reduction power of the most active strains and the reduction efficiency of selenite was defined and calculated.

The reduction power of *F.oxysporum* decreased by increasing the selenium concentration, it reached the maximum value 96.6% at 1mM concentration of sodium selenite, while the reduction power of *R. mucilaginosa* and *C. albidus* reached the maximum value 99 and 98.8% at 5 and 7mM of sodium selenite respectively and decreased above this concentration which may be due to selenite toxicity, and this result is similar to that obtained by **(Golubev *et al*., 2001)**, who noted that as selenium concentrations were increased, the number of yeasts that could grow at a given concentration sharply decreased. Fungal growth was often inhibited together with the reduction of $SeO3^{-2}$ to Se^0 **(Gharieb *et al*., 1995, 1999)**. The reduction is caused by fungi's capacity to secrete metabolic substances including phenolic, flavonoids, and tannins or reductase enzymes that serve as selenium ion electron donors and convert them into atoms **(Lokanadhan *et al*., 2019).** The high concentrations of selenite activate toxification processes **(Kousha *et al*., 2017).** Some of the primary processes by which fungus produce nanoparticles and nanominerals. Nanomaterials can develop intracellularly, extracellularly, in reaction culture filtrates devoid of biomass, on dead biomass, and in association with cell walls and surface

materials. Metal (loid) species may sorb to cell walls and EPS, giving mineral nucleation sites in the process. The type of nanomaterials produced can be influenced by redox processes, the presence of ligands, metabolites, and organic molecules, among other factors. Amino acids, proteins, and byproducts of autolysis that are secreted can affect the size and development of newly produced nanomaterials. Some ligands, such phosphate, carbonate, and sulphur dioxide, may be produced by the metabolism of some fungi and the dissolution of certain minerals. Metal (loid) transport through the plasma membrane can lead to redox transformations of accumulating metal (loid) species, sequestration by intracellular macromolecules such metallothionein and phytochelatins, and intracellular vacuolar compartmentation **(Qianwei *et al.*, 2022)**.

The generated nanoparticles were spherical in shape, as seen by the TEM photographs of the synthesized nanoparticles. The particles ranged in size from 14 to 97 nm. Additionally, the selenium content of the nanoparticles is confirmed by the EDX spectrum. The protein molecules can be identified by the additional carbon and oxygen peaks. These results are compared with **(Sarker *et al.*, 2011),** the production of mono dispersion spherical-selenium nanoparticles in the range of 30 to 150 nm was explained by transmission electron microscopic images. Our findings showed that these strains may create selenium nanoparticles with a narrower particle size distribution and a smaller average nanoparticle size. It may be inferred from the overall results of the FTIR investigation that the proteins may have formed a capping agent over the SeNPs, which may have contributed to their stabilization. The existence of a protein shell outside the nanoparticles was confirmed by Fourier transform infrared spectroscopy, which in turn supports their stabilization **(Sarker*et al.*, 2011)**.It is generally known that free amine groups, cysteine residues, and protein can bind to selenium nanoparticles, stabilizing SeNPs by surface-bound protein may be a possibility, limiting agglomeration and showing potential for medical activity **(El-Deeb *et al.*, 2018).** It is noteworthy that the connection between Se nanoparticles and proteins is just electrostatic between the selenium atoms, NH and C = O groups **(Zhang *et al.*, 2011)**. In particular, Lenz and co-workers **(Lenz *et al.*, 2011)** showed that a variety of high-affinity proteins can bind to selenium nanoparticles.

The resonance peak of selenium nanoparticles is confirmed by numerous

publications to be in the 200–300 area, but the precise location relies on a number of variables, including particle size, shape, and material composition, as well as the immediate environment **(Sarker *et al.*, 2011)**.There were a lot of study about SeNPs formation have various absorption peaks in UV-vis spectra indicate to a presence ofSeNPs. In these studies, the peaks appeared at 238, 240 and 245 nm which corresponds to the particle size of 14-97 nm **(El-Deeb *et al*., 2018)**.

Conclusion

In conclusion, these studies might suggest that some unicellular and multicellular fungi have the ability to produce SeNPs intracellulary and extra cellulary respectively, with an environmentally friendly and safe method.

Acknowledgements

I would gratefully acknowledge, Dr. Ibrahim Elsayed Mousa, Microbiology, Environmental Biotechnology department, Genetic Engineering and biotechnology Research institute (GEBRI), Menoufia University.

References:

Ashengroph M., and Hosseini S. R, (2021). A newly isolated *Bacillus amyloliquefaciens* SRB04 for the synthesis of selenium nanoparticles with potential antibacterial properties. *Int. Microbiol*., 24:103-114.

Aksu Z., and Eren A. T, (2005). Carotenoids production by the yeast *Rhodotorula mucilaginosa*: use of agricultural wastes as a carbon source. *Process Biochem.* 40: 2985–2991. doi: 10.1016/j.procbio.2005.01.011.

Avendaño R., Chaves N., Fuentes P., Sánchez E., Jiménez J. I., and Chavarría M, (2016). Production of selenium nanoparticles in *Pseudomonas putida* KT2440. *Scientific reports*. 6: 37155.

Bajaj M., Schmidt S., and Winter J, (2012). Formation of Se (0) Nanoparticles by *Duganella* sp. And *Agrobacterium* sp. isolated from Se-laden soil of North-East Punjab, India. *Microbial cell factories.* 11(1): 64.

Barrnett J. A., Payne R. A., and Yarrow D, (1990). Yeast characteristics and identification (2nd edition) Cambridge Universitypress, Cambridge.

Bartůněk V., Junková J., Šuman J., Kolářová K., Rimpelová S., Ulbrich P., and Sofer Z, (2015). Preparation of amorphous antimicrobial selenium nanoparticles stabilized by odor suppressing surfactant polysorbate 20. *Materials Lett*., 152: 207-209.

Combs G. F., and Gray W. P, **(1998).** Chemopreventive Agents: Selenium, *Pharmacol. Thera*p., 79(3):179–192.

Dhanjal S., and Cameotra S. S, (2010). Aerobic biogenesis of selenium nanospheres by *Bacillus cereus* isolated from coalmine soil**.** *Microb. Cell Fact*., 52 (9):1-11.

Díaz-Visurraga J., Daza C., Pozo C., Becerra A., von Plessing C., and García A., (2012). Study on antibacterial alginate-stabilized copper nanoparticles by FT-IR and

2D-IR correlation spectroscopy. *Inter. J. Nanomedicine*. 7: 3597-3612.

El-Deeb B., Al-Talhi A., Mostafa N., and Abou-assy R, (2018). Biological Synthesis and Structural Characterization of Selenium Nanoparticles and Assessment of Their Antimicrobial Properties. *A. S. R.J.* 45(1): 135-170.

Gharieb M. M., Kierans M., and Gadd G. M., (1999). Transformation and tolerance of tellurite by filamentous fungi: accumulation, reduction, and volatilization. *Mycol. Res.*, 103:299–305.

Gharieb M. M., Wilkinson S. C., and Gadd G. M, (1995). Reduction of selenium oxyanions by unicellular, polymorphic and filamentous fungi: cellular location of reduced selenium and implications for tolerance. *J.Ind.Microbiol.*, 14:300–311.

Ghosh A., Mohod A. M., Paknikar K. M., and Jain R. K, (2008). Isolation and characterization of selenite-and selenate-tolerant microorganisms from selenium-contaminated sites. *W.J. M. B.* 24(8): 1607-1611.

Golubev V. I., and Golubev N. V,(2001). Selenium tolerance of yeasts, *Microbiology*, Vol. 71, No. 4, 2002, pp. 386–390. Translated from Mikrobiologiya, 71(4): 455–459.

Harrigan W. F, (1998). Laboratory methods in food microbiology. San Diego. *Appl. Microbiol. Biotechnol.*, 103: 7241-7259.

Huang J., Li Q., Sun D., Lu Y., Su Y., Yang X., and Hong J, (2007). Biosynthesis of silver and gold nanoparticles by novel sundried Cinnamomumcamphora leaf. *Nanotechnology*. 18(10): 105104. *IET Nanobiotechnol*., 13: 214-218.

Knekt P., Marniemi J., Teppo L., Heliovaara M., and Aromaa A, (1998). Is low selenium status a risk factor for lung cancer. *A.J.E.* 148: 975-982.

Korhola M., Vainio A., and Edelmann K, (1986). Selenium Yeast, *Ann. Clin. Res*., 18(1): 65–68.

Kousha M., Yeganeh S., and Amirkolaie A. K, (2017). Effect of sodium selenite on the bacteria growth, selenium accumulation, and selenium biotransformation in *Pediococcus acidilactici*. *F.S.b*. 26(4): 1013-1018.

Kurtzman P. C., fell J. W., Boekhout T., and Robert V, (2011).Methods for isolation, phenotypic characterization and maintainance of yeast. In the yeast, a taxonomic study. Vol 1, 5th, ed, *Elsevier, Amsterdam.*

Lenz M., Kolvenbach B., Gygax B., Moes S., and Corvini P. F, (2011). Shedding light on selenium biomineralization: proteins associated with bionanominerals. *A.E.M.* 77(13): 4676-4680.

Li Q., Chen T., Yang F., Liu j., and Zheng w, (2010). Facile and controllable one-step fabrication of selenium nanoparticles assisted by l-cysteine. *Materials Letters*, 64: 614-617.

Lodder J, (1970). The yeast: Taxonomic study (2nd edition) North Holand Publ., Crop Amsterdam, London.

Lokanadhan G., Dass R. S., and Kalagatur N K, (2019). Phytofabrication of Selenium Nanoparticles from Emblicaofficinalis fruit extract and exploring its biopotential applications: Antioxidant,

Antimicrobial, and Biocompatibility. *F.M.* 10: 931.

Mannazzu I., Landolfo S., Lopes da Silva T., and Buzzini P., (2015). Red yeasts and carotenoid production: outlining a future for non-conventional yeasts of biotechnological interest. *W.J.M.B.* 31, 1665–1673. doi: 10.1007/s11274-015-1927-x.

Mashreghi M., and Shoeibi S., (2017). Biosynthesis of selenium nanoparticles using *Enterococcus faecalis* and evaluation of their antibacterial activities. *J.t.e.m.b.* 9, 003.

Medina Cruz D., Mi G., and Webster T., J., (2018). Synthesis and characterization of biogenic selenium nanoparticles with antimicrobial properties made by *Staphylococcus aureus, methicillin-resistant Staphylococcus aureus* (MRSA), *Escherichia coli*, and *Pseudomonas aeruginosa. J. B.M.*. A, 106, pp. 1400-1412.

Mukherje M, (2014). In vitro antimicrobial activity of polyacrylamide doped magnetic iron oxide nanoparticles. *I.J.M. Ma. Man.* 2(2): 64-66.

Prasad K. S., and Selvaraj K, (2014). Biogenic synthesis of selenium nanoparticles and their effect on As (III)-induced toxicity on human lymphocytes. *Biological trace element research*. 157(3): 275-283.

Qianwei Li., Feixue Liu., Chunmao Chen., and Geoffrey Michael Gadd, (2022). Nanoparticle and nanomineral production by fungi. Geomicrobiology Group, School of Life Sciences, University of Dundee, DD1 5EH, Scotland, UK, Volume 41.

Rajendran D., (2013). Aplication of nanominerales in animal production system. *Res. J. Biotechnol*., 8 (3): 1-3.

Ramamurthy C. H., Sampath K. S., Arunkumar P., Kumar M. S., Sujatha V., Premkumar K. and Thirunavukkarasu C, (2013). Green synthesis and characterization of selenium nanoparticles and its augmented cytotoxicity with doxorubicin on cancer cells. *B.J.b.e.* 36(8): 1131-1139.

Ramya S., Shanmugasundaram T., and Balagurunathan R, (2018). Biomedical potential of actinobacterially synthesized selenium nanoparticles with special reference to anti-biofilm, anti-oxidant, wound healing, cytotoxic and anti-viral activities. *J. T. E. M.B.*, 32: 30-39.

Salem E. Z., Shahin I. M., Yaser F. M., Hamed M. A., Abdel Hamid M. F., and Emam H., (2010). Applicability of Fourier transform infrared (FTIR) spectroscopy for rapid identification of some yeasts and dermatophytes isolated from superficial fungal infections. *J.E.W.D.* 7: 105-110.

Sarkar J., Dey P., Saha S., and Acharya k,(2011). Molecular and Applied Mycology and Plant Pathology Laboratory, Department of Botany, University of Calcutta, Kolkata 700019, India.

Sharma R., and Ghoshal G, (2020). Optimization of carotenoids production by *Rhodotorula mucilaginosa* (MTCC-1403) using agro-industrial waste in bioreactor: a statistical approach. *Biotechnol. Rep.* 25, e00407. doi: 10.1016/j.btre.2019.e00407.

Singh N., Saha P., Rajkumar K., and Abraham J., (2014). Biosynthesis of

silver and selenium nanoparticles by *Bacillus* sp. JAPSK2 and evaluation of antimicrobial activity. *Der Pharmacia Lett.,* 6(6): 175-181.

Sonkusre P., Nanduri R., Gupta P., and Cameotra S. S, (2014). Improved extraction of intracellular biogenic selenium nanoparticles and their specificity for cancer chemoprevention. *J.N.N*. 5(2):1.

Srivastava N., and Mukhopadhyay M, (2015). Green synthesis and structural characterization of selenium nanoparticles and assessment of their antimicrobial property. Bioprocess and biosystems engineering. 38(9): 1723-1730.

Tani A., Kato S., Kajii Y., Wilkinson M., Owen S., and Hewitt N, (2007). A proton transfer reaction mass spectrometry based system for determining plant uptake of volatile organic compounds. *Atmospheric Environment*. 41(8): 1736-1746.

Xin Zhang., Wen Yuan Fan., Mu Cenyao., Chuan Wang Yang., and GuoPingsheng, (2020). Redox state of microbial extracellular polymeric substances regulates reduction of selenite to elemental selenium. Vol 172, 115538.

Zayed M., and Badawi M. A., **(2020**). In-Silico Evaluation of a New Gene from Wheat Reveals the Divergent Evolution of the CAP160 Homologous Genes Into Monocots. *J. Mol. Evol.* , 88: 151–163.

Zhanga W., Chena Z., Liua H., Zhangb L., Gaoa P., and Li D, (2011). Biosynthesis and structural characteristics of selenium nanoparticles by *Pseudomonas alcaliphila* Colloids Surf. B: *Biointerfaces,* 88: 196-202.

Zonaro E., Piacenza E., Presentato A., Monti F., Dell'Anna R., and Lampis S., Vallini G, (2017). *Ochrobactrum* sp. MPV1 from a dump of roasted pyrites can be exploited as bacterial catalyst for the biogenesis of selenium and tellurium nanoparticles. *Microb. Cell. Fact*., 16, p. 215.

التخليق الحيوي الداخلي والخارجي لجسيمات السيلينيوم النانوية عن طريق الفطريات أحادية الخلية والخيطية التي تتحمل السيلينيوم

محمد مدحت غريب، عزه محمود سليمان و اسراء محمد حسان

قسم الميكروبيولوجى - كلية العلوم – جامعة المنوفية

يهدف البحث الى تخليق جزيئات السيلينيوم النانونيه بواسطه بعض الفطريات الاحاديه والخيطيه بطريقه امنه علي البيئه وبالتالي تم عزل ٥٠ نوع من الفطريات الاحاديه والخيطيه معا من اماكن مختلفه واختبار قدرتها علي اختزال سيلينات الصوديوم وتحويلها الي جزيئات السيلينيوم في صوره نانونيه. وقد وجد ان ٢٨ نوع فقط من هذه العزلات لهم القدره علي اختزال سيلينات الصوديوم وتحويلها الي جزيئات السيلينيوم في الصوره النانونيه ، لذلك تم اختبار قدره هذه الفطريات علي تحمل التركيزات العاليه من سيلينات الصوديوم وتحويلها لجزيئات السيلينيوم النانونيه عند فترات تحضين مختلفه. وقد تم اختيار العزلات الاكثر نشاطا وتحملا لتركيزات السيلينيوم المرتفعه وتعريفها علي اسس فسيولوجيه وجزيئيه وتبين انهما

Fusarium oxysporum, Rhodotorula mucilaginosa and *Cryptococcus albidus*.

وبالتالي تم اختيار هذه الفطريات لمزيد من الدراسه. وتم توفير افضل الظروف لهذه الفطريات للحصول علي اعلي نسبه لاختزال سيلينات الصوديوم تبين ان قوة الاختزال لل *Fusarium oxysporum* انخفضت بزيادة تركيز السيلينات خارج الخليه ، ووصلت إلى القيمة القصوى ٩٦.٦٪ من تركيز ١ ملي مولار من سيلينات الصوديوم مع الوزن الجاف الصافي ٧.٧ مجم / مل. ومع ذلك ، فإن قوة الاختزال لـ *Rhodotorula mucilaginosa* ، *Cryptococcus albidus* داخل الخليه وصلت إلى أقصى قيمة ٩٩ و ٩٨.٨٪ من ٥ و ٧ ملي مولار من سيلينات الصوديوم مع صافي الوزن الجاف ٧.٢ و ٦.٦ مجم / مل على التوالي. تمت تنقية جزيئات السيلينيوم المُصنَّعة حيوياً وتجفيفها عند ٤٠ درجة مئوية ، وتم تمييزها باستخدام التحليل الطيفي للأشعة فوق البنفسجية ، والتحليل المجهري الإلكتروني و تحليل الطيف بالأشعة تحت الحمراء (FTIR) ، وذلك لتأكيد تكوين جزيئات السيلينيوم النانوية.

أوضحت الصور المجهرية الإلكترونية تشكيل جزيئات نانونية كروية أحادية التشتت في نطاق ١٤-٩٧ نانومتر مع شكل كروي . بالإضافة إلى ذلك ، ظهرت ذروة الرنين عند ٢٠٠-٣٠٠ نانومتر وهو ما يتوافق مع حجم الجسيمات ١٤-٩٧ نانومتر. أكد التحليل الطيفي بالأشعة تحت الحمراء وجود غلاف بروتيني خارج الجسيمات النانوية.